Analyst

Accepted Manuscript

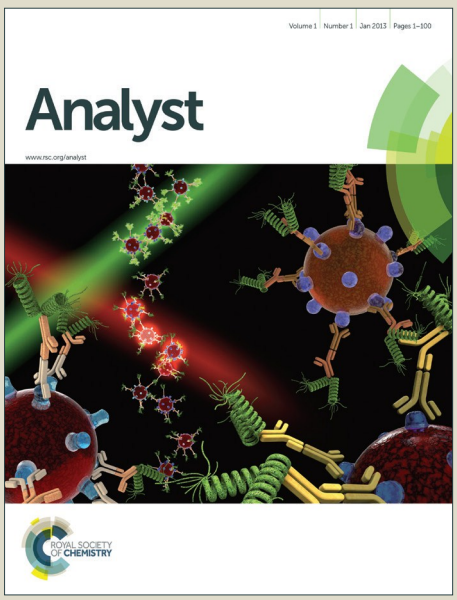

ROYAL SOCIETY OF CHEMISTRY

www.rsc.org/analyst

Journal Name

ARTICLE

Microfluidic compartments with sensing microbeads for dynamic monitoring of cytokine and exosome release from single cells

Received 00th January 20xx,
Accepted 00th January 20xx

DOI: 10.1039/x0xx00000x

www.rsc.org/

Kyung Jin Son[a], Ali Rahimian[a], Dong-Sik Shin[a,c], Christian Siltanen[a], Tushar Patel[b] and Alexander Revzin[a,†]

Monitoring activity of single cells has high significance for basic science and diagnostic applications. Here we describe a reconfigurable microfluidic device for confining single cells along with antibody-modified sensing beads inside 20 picoliter (pL) microcompartments for monitoring cellular secretory activity. An array of ~7000 microchmabers fabricated in the roof of the reconfigurable microfluidic device could be raised or lowered by applying negative pressure. The floor of the device was micropatterned to contain cell attachment sites in registration with the microcompartments. Using this set-up, we demonstrated detection of inflammatory cytokine IFN-γ and exosomes from single immune cells and cancer cells respectively. The detection scheme was similar in both cases: cells were first captured on the surface inside the microfluidic device, then sensing microbeads were introduced into the device so that, once the microcompartments were lowered, single cells and microbeads became confined together. The liquid bathing the beads and the cells inside the compartments also contained fluorescently-labeled secondary antibodies (Abs). The capture of cell-secreted molecules onto microbeads was followed by binding of secondary antibodies – this caused microbeads to become fluorescent. The fluorescence intensity of the microbeads changed over time, providing dynamics of single cell secretory activity. The microdevice described here may be particularly useful in the cases where panning upstream of sensing is required or to analyze secretory activity of anchorage-dependent cells.

Introduction

Traditional cell ensemble measurements mask functional and phenotypic heterogeneities among cell populations, which is critical for comprehensive understanding of cellular networks[1-3]. In particular, secretory activities of individual cells may correlate with pathological developments and may provide important information for disease diagnosis. Therefore, analysis of single cellular secretory activities has drawn tremendous interest from biology/medicine researchers in recent years. Enzyme-linked immunospot (ELISpot) assay, relying on a colorimetric enzymatic reaction of antibodies, is one of the most extensively used methods for measuring the cellular secretory activities *in vitro*[4]. Although ELISpot is sensitive enough to detect low frequency single cells, this assay does not provide temporal information about cell secretions. In addition, it utilizes large volumes of cells and reagents. The flow cytometry combined with intracellular staining is another traditional means of detecting protein expression at the single cell level. However, this approach is not compatible with live cells and reports on intracellular accumulation rather than secretion of molecules. Micro- and nano-technology approaches are particularly well suited for single cell analysis. A number of approaches including microwells[5-7], droplets[8], traps[9], and tubes[10] have been developed for capture and analysis of single cells. In addition, it is possible to retrieve desired single cells from devices by various means[11-15]. Of particular note is the prior work aimed at developing microcompartments for capturing single cells in proximity of antibodies (Ab) specific to cell-secreted signals[16-18]. While any secreted protein may be detected using this method, these devices focused on profiling cytokine secretions from single immune cells. Cytokine capture Ab molecules were either immobilized in the array form[16, 18] or were uniformly distributed on the surface on the cell capture compartment[17]. After cell secretion experiment the devices were stained with secondary antibodies to reveal presence of captured cytokines. While very useful, this strategy for single cell analysis offers limited temporal information about cell secretion.

[a]*Department of Biomedical Engineering, University of California, Davis, Davis, California, 95616, USA*
[b]*Department of Cancer Biology, Mayo Clinic, Jacksonville, Florida, 32224, USA*
[c]*Department of Medical & Pharmaceutical Sciences, Sookmyung Women's University, Seoul, Korea*
† Corresponding author. arevzin@ucdavis.edu
Electronic Supplementary Information (ESI) available: [details of any supplementary information available should be included here]. See DOI: 10.1039/x0xx00000x

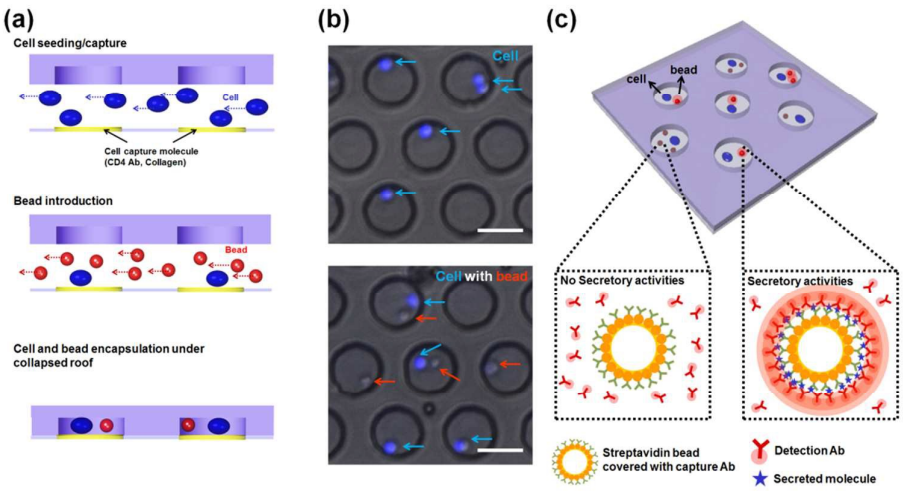

Fig. 1 Microcompartment arrays for isolating single cells and sensing beads for monitoring cellular secretory activity. (a) Drawing of the reconfigurable microfluidic device, and (b) microscope images showing cells and cells with sensing beads encapsulated inside the compartment. Blue arrows and red arrows in (b) indicate cells stained with CellTracker and beads, respectively. Scale bar = 30 µm. (c) Individual compartment consisting of single cells and sensing beads surrounded by PE-labelled detection antibodies as reporter molecules. Once released by cells, target molecules diffused inside the chamber, bound to sensing bead, causing fluorescence increase on bead surface via sandwich assay.

Another strategy for single cell analysis is to encapsulate single cells inside microdroplets alongside Ab-functionalized microbeads and fluorescently labeled secondary Abs[8, 19, 20]. Secreted molecules become captured on microbeads; this in turn leads to binding of secondary Abs and appearance of fluorescence signal. Importantly, the signal appears dynamically without the need for secondary labeling or staining. While encapsulating cells inside droplets is exciting, there may be applications that benefit from having cells bind to surfaces prior to analysis, for example those involving anchorage dependent cells or those requiring isolation of specific cellular subsets from a heterogeneous mixture.

Previously, our lab has developed reconfigurable microfluidic compartments that were used in conjunction with peptide-modified hydrogel structures for monitoring protease release from single cells[14]. However, this previous device relied on the proteolytic cleavage of peptides for generating the signal and was not easily adaptable to the detection of other types of secreted molecules. In the present study, we describe a more general strategy for monitoring single cell secretions by combining reconfigurable microcompartments and Ab-modified microbeads. The principle of operation of the device is shown in Fig. 1. The microcompartments were molded in the roof of the reconfigurable microfluidic device. The roof may be raised or lowered by applying and releasing negative pressure, thus opening or closing compartments. Cells are captured on the micropatterned floor of the device after which microbeads are flowed into the device and become entrapped inside the compartments upon actuation of the reconfigurable microfluidic device. In addition to single cells and microbeads, compartments contained free-floating fluorescent secondary Abs. Microbeads captured cell-secreted molecules and became fluorescent upon binding of secondary Ab molecules from solution (Fig. 1). One demonstration of this microsystem was to capture single CD4 T-cells and monitor release of interferon (IFN)-γ over time. Analysis of IFN-γ release from CD4 T-cells is used clinically for diagnosis of TB exposure[21] and being able to dynamically monitor release of this cytokine may provide valuable information about this disease. In another demonstration, this microsystem was used for detection of exosome release from hepatocellular carcinoma (HCC) cells. Exosomes are nanovesicles (diameter: 30 – 150 nm) secreted by a variety of healthy and malignant cell types [22-25] and have recently garnered attention for their diagnostic potential[26-28]. The microsystem developed here allowed us to monitor exosome release dynamically with single cell resolution. Overall, this paper describes a general strategy for dynamic monitoring of secretory activity from single cells. It may be combined in the future with cell retrieval approaches to enable function-based sorting of single cells.

Materials and Methods

A. Materials

Streptavidin coated polystyrene particles (diameter = 5.0 – 5.9 µm) were obtained from Spherotech (Lake Forest, IL). Biotinylated rabbit anti-human CD63 antibodies (anti-CD63 Ab-biotin) and PE-conjugated rabbit anti-human CD63 antibodies (anti-CD63 Ab-PE) were purchased from Bioss (Woburn, MA). Biotinylated goat anti-human IFNγ antibodies (anti-IFNγ-biotin), PE-conjugated mouse anti-human IFNγ antibodies (anti-IFNγ-PE) and Alexa 488-conjugated anti-human IFNγ antibodies (anti-IFNγ-488) were purchased from R&D Systems (Minneapolis, MN). Mouse anti-human CD4 antibodies (anti-CD4 Ab) were obtained from Beckman Coulter (Miami, FL). CellTracker™ Blue CMAC Dye was purchased from Thermo Fisher Scientific, Inc. (Waltham, MA).

Phorbol 12-myristate 13-acetate (PMA) and ionomycin were obtained from Sigma-Aldrich. Phosphate buffered saline (PBS) was purchased from TEKnova (Hollister, CA). Glass slides (75 × 25 mm^2) and cover glasses (24×30×0.13 mm) were from

Fisher Scientific (Pittsburgh, PA). All other chemicals were purchased from Sigma (St. Louis, MO) or Aldrich Chemicals (Milwaukee, WI). MATLAB (MathWorks Inc., Natick, MA) and COMSOL Multiphysics (COMSOL, Inc., Burlington, MA) were used for modeling of antibody binding, and calculating the cellular secretion rates.

$CD4^+$ T cells were isolated (cell purity = ~ 95%) from human PBMCs drawn from healthy donors by negative selection using Human $CD4^+$ T Cell Enrichment Kit (Stemcell Technologies, Vancouver, BC, Canada) according to the manufactures instructions, and cultured in serum-free X-Vivo 15 medium with Gentamicin (Lonza, Walkersville, MD) and 1% (v/v) penicillin-streptomycin at 37 °C in a humidified 5% CO_2 atmosphere. The stimulation of $CD4^+$ T cells was carried out by PMA (50 ng mL^{-1}) and Ionomycin (1μg mL^{-1}). A human hepato carcinoma cell line, HepG2 (American Type Culture Collection (ATCC), Manassas, VA) were cultured in EMEM (Eagle's Essential Minimum Medium, ATCC, Manassas, VA) medium supplemented with 10% (v/v) fetal bovine serum and 1% (v/v) penicillin-streptomycin at 37 °C in a humidified 5% CO_2 atmosphere. Exosomes derived from HepG2 cells were isolated from the supernatant of 24 h FBS starved cultured cells utilizing ExoQuick reagent (System Bio Sciences, Mountain view, CA), and Amicon Ultra-15 centrifugal filters (EMD Millipore, Billerica, MA). The supernatant was clarified by vacuum filtration using the Steriflip® filter unit 0.22 μm Millipore Express PLUS (PES) membrane (EMD Millipore, Billerica, MA). Then the samples were concentrated by centrifugation at 3000g for 30 minutes in Amicon ultra-15 centrifugal filters at 4°C, then buffer exchanged with PBS through an extra centrifugation step with the same setting, then incubated overnight with ExoQuick at 4°C. After 16 h of incubation the solutions were centrifuged at 1500g for 30 minutes at 4°C. The pellet containing the exosomes was re-suspended in PBS. BCA protein assay (Life Technologies, Grand Island, NY), and Zeta Potential/Particle Sizer (PSS.NICOMP-Particle sizing systems, Santa Barbara, CA) were used to evaluate the quality of isolated particles. A cell culture chamber was built on a Nikon eclipse Ti fluorescence microscope (Nikon Instruments, Inc.) for live-cell analysis, maintaining the environmental conditions for optimal growth and functioning of cells during experiment. The temperature of our device was controlled by Tokai Hit Thermo-E microscope heating stage (Tokai Hit, Japan) while 5% CO_2 was supplied to the incubator.

B. Preparation of antibody-functionalized microbeads

Streptavidin-coated microbeads were used as reporters for cellular secretory activities by being functionalized with biotinylated capture antibodies through biotin-streptavidin interactions. Prior to functionalization, microbeads were washed with PBS three times via a centrifugation (at 10,000 rcf for 2 min, Centrifuge 5424, Eppendorf, Hambrug, Germany)/washing protocol. 0.1mg of streptavidin-microbeads (~1.4×10^6 beads) were incubated with 30 μL of biotinylated capture antibodies (0.05 mg mL^{-1} in PBS) for 2 h at room temperature or overnight at 4°C, followed by rinsing with PBS by a centrifugation/washing protocol. After blocking with 1% BSA for 30 min at room temperature, antibody-microbeads were used immediately or stored for up to 2 weeks at 4°C.

C. Fabrication of reconfigurable microfluidic device

Reconfigurable microfluidic device having a reversibly collapsible array of subpicoliter chambers was prepared via a multilayer soft lithography as described in previous reports[29, 30]. Briefly, the pre-polymer solution of polydimethylsiloxane (PDMS; Sylgard 184, Dow Corning), mixed at a 10: 1 curing (weight) ratio, was poured onto a photoresist patterned substrate and placed under vacuum to remove air bubbles. The two-layer microfluidic device is composed of a bottom flow layer (400 μm thickness) and a top control layer (1 cm thick). The control layer was baked first for 30 minutes at 70°C, and the flow layer was baked for 20 minutes while holes were punched for the control layer. Then, the two layers were carefully aligned by eye and adhered together. Finally, the devices were baked for one hour to become fully cured. Afterward, the devices were cut out and used for experiments. It is well-known that PDMS is permeable to gases including oxygen but is impermeable to proteins. To reduce nonspecific binding of proteins to the PDMS surface, we blocked the surface with 1% bovine serum albumin (BSA) for 1 h at room temperature before experiments.

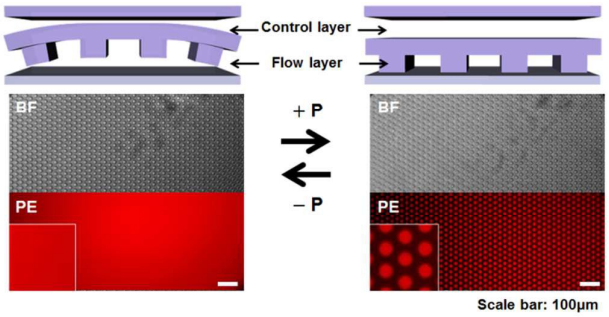

Fig. 2 Drawing of the reconfigurable microfluidic device (upper images), and optic/fluorescence images (lower images) illustrating the working principle using red fluorophore, PE.

The working principle of a reconfigurable device is described in Fig. 2. When vacuum is applied to the upper flow layer of device, the reversibly collapsible flow layer is raised and red fluorophore is distributed throughout (open configuration). On the other hand, when vacuum is released and positive pressure is applied to the upper flow layer (close configuration), the flow layer descended from roof to the substrate, generating an array of compartments with a volume of ~ 20 pL that limits the diffusion of analytes between chambers, and amplifying the signal.

D. Surface patterning with cell capture moieties

The glass substrates were cleaned in an oxygen plasma chamber (YES-R3, San Jose, CA, USA) at 300 W for 15 min and then incubated in 3% (v/v) 3-aminopropyltriethoxysilane (APTES) in absolute ethanol for 2 h at room temperature in the moisture-controlled environment. The slides were flushed with fresh ethanol to remove non-covalently bound APTES, dried under nitrogen, and then cured at 100°C for 2 h. Then, the slides were further incubated in 2.5% (v/v) glutaraldehyde (GA) in PBS for 2 h at room temperature, followed by rinsing with DI water and dried under nitrogen. GA-modified substrates were used immediately or placed in a desiccator until future use. To

define the site for cell attachment, the GA-modified surfaces were patterned with cell capture moieties using our reconfigurable microfluidic devices (FIG. S-1(a)). For cytokine detection from T cells, anti-CD4 Abs (0.2 mg mL^{-1}) were used as cell capture moieties, while collagen I (0.1 mg mL^{-1}, BD Biosciences, San Jose, CA) being used for exosome detection from HepG2 cells. Once a reconfigurable microfluidic device was aligned over the GA-modified slides, the vacuum was applied to the control layer (open configuration), facilitating flow-in of cell capture moieties. Then, vacuum was released so that the flow layer with a chamber array descended on the slide (close configuration), keeping a solution of cell capture moieties inside the confined chambers for 1.5 h at room temperature. After rinsing with PBS in the open configuration, the surface was blocked with 1% BSA for 1 h at room temperature to prevent nonspecific binding of cells. The presence of cell capture moieties patterns on surface was verified using PE-labelled secondary antibodies verifying that the size of cell capture moiety patterns is similar to that of mocrocompartments (diameter = 30 μm for T cells and 40 μm for HepG2 cells) as shown in FIG. S-1(b).

E. Constructing calibration curves for IFN-γ and exosomes

To assess signal vs. analyte concentration relationship, calibration curves were generated by challenging antibody-microbeads with different concentrations of recombinant cytokines or isolated exosomes. First, microbeads functionalized with IFN-γ capture (c)Ab (5.68×10^5 particles) were exposed to 20 μL of solution containing PE-labelled detection (d)Abs (25 μg mL^{-1}) as well as recombinant IFN-γ (with various concentrations ranging from 0 to 200 ng mL^{-1}) in the 0.5 mL tube, and immediately, infused into the microfluidic device. The saturated fluorescence signals from microbeads were detected at t = 60 min. Similarly, exosome cAbs (anti-CD63 Abs) containing microbeads (2×10^4 particles) were challenged to 20 μL of solution containing PE-labelled dAbs (25 μg mL^{-1}) and isolated exosomes (0 – 60 ng mL^{-1}) in the 0.5 mL tube, and infused to the microfluidic device. Isolated exosomes, more specifically the protein content of exosomes, were quantitated by BCA protein assay kit. Even though the concentration determined by BCA assay refers the protein content of exosomes rather than exosomes themselves, BCA assay has been used to provide information on the quantity of isolated exosomes[31, 32]. Fluorescence signals were observed for 3 h.

F. Cell capture and detection

A reconfigurable microfluidic device with the cell capture moieties-patterned substrate was employed for real time monitoring of single cellular secretory activities. It is of note that the single cell trapping efficiency inside the microfluidics depends on cell density as well as flow rate and the optimal conditions for cell density or flow rate depend on the cell type. Compared to suspension cells, adherent cells were seeded with a lower density at a higher flow rate to achieve higher single cell capture efficiency.

To detect cytokine secretion from T cells, cells suspended in serum-free X-vivo medium (~1×10^6 cells mL^{-1}) were infused into the device in open configuration at 2 μL min^{-1} for 60 min. Unbound T cells were removed by washing with serum-free medium at 25 μL min^{-1} for 30 min. Subsequently, antibody-microbeads (2.84×10^7 particles mL^{-1}) and PE-labelled detection antibodies (25 μg mL^{-1}) suspended in mitogenic solution containing 50 ng mL^{-1} of PMA and 1 μg mL^{-1} of Ionomycin in serum-free X-vivo medium were introduced into the channel at 10 μL min^{-1} for 5 min. After the control layer of the microfluidic device was collapsed (closed configuration), time-lapse images of fluorescence signals on antibody-microbeads were acquired at 30 min intervals for a total of 6 h at exposure time of 0.2 msec. The viability of T cells encapsulated in bead containing chambers during the measurement was confirmed using LIVE/DEAD viability/cytotoxicity assay as shown in FIG. S-2.

In a similar manner, we also monitored the exosome production from HepG2 cells. HepG2 cells were suspended in serum-free EMEM medium with a concentration of 1×10^5 cells mL^{-1} and introduced into the device in open configuration at 5 μL min^{-1} for 20 min, followed by washing unbound cells with serum-free medium at 25 μL min^{-1} for 30 min. Antibody-microbeads (2.84×10^7 particles mL^{-1}) and PE-labelled detection antibodies (25 μg mL^{-1}) suspended in serum-free medium were injected into the channel at 10 μL min^{-1} for 5 min, and fluorescence signals on microbeads encapsulating with cells in chambers were monitored in the close configuration of device. Time-lapse images of sensing chamber arrays were acquired at 30 min intervals for a total of 12 h at exposure time of 0.2 msec. We carried out control experiments and determined that fluorescent antibodies were not photobleached during microscopy observation.

Results and Discussion

This paper describes a reconfigurable microfluidic device integrated with sensing microbeads to enable dynamic monitoring of cell-secreted molecules at the single cell level. Detection of IFN-γ from individual CD4 T-cells and exosomes from single hepatocellular carcinoma cells was demonstrated.

A. Antibody-functionalized microbeads as sensing elements

In the current study, we utilized streptavidin-coated microbeads as sensing elements for monitoring cellular secretory activities. Any biotinylated biomolecules (e.g.

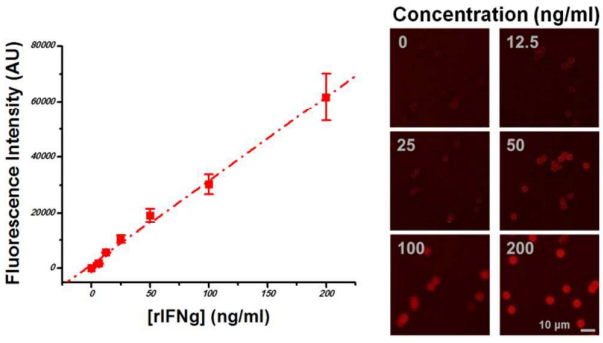

Fig. 3 Fluorescence intensities of anti-IFN-γ cAb-beads after incubating with different concentrations of recombinant human IFN-γ (conc. = 0 – 200 ng mL^{-1}) and PE-labelled anti-IFN-γ dAb (conc. = 5 μg mL^{-1}) for 60 min, verifying cytokine detectability using anti-IFN-γ cAb-beads.

antibodies, peptides, or aptamers) can be conjugated onto microbeads via streptavidin-biotin interaction. Microbeads are also advantageous from the standpoint of offering larger surface area for loading capture antibodies. For example, a microbead with diameter of 5 μm (typically used in our experiments) has a surface are of 78.5 μm^2 whereas flat surface with the same diameter has an area of 19.6 μm^2. Prior to engaging in cell analysis, we characterized signal vs. analyte concentration relationship (Fig. 3). In these experiments, microbeads conjugated with IFN-γ cAbs were exposed to various concentrations of recombinant IFN-γ ranging from 0 to 200 ng mL^{-1} inside the microfluidic device. The fluorescence signal was created by incubating microbeads with PE-labelled dAb. The calibration curve shown was used to determine that linear range of the biosensor extended to 200 ng mL^{-1}. The limit of detection (LOD) was determined to be 21.4 ng mL^{-1} based on signal-to-noise characteristics (S/N = 3)[33], while notable signal was observed from 12.5 ng mL^{-1} of recombinant IFN-γ. The binding capacity of Ab-functionalized microbeads is one of the most critical factors, not only determining the lifespan of the sensor but also having an influence on the conservation equation which will used for numerical simulation in following sections. We conducted ELISA (Enzyme-linked immunosorbent assay) experiment as well as fluorescence-based sandwich assay in order to determine the binding capacity, which is one of the important parameters for simulation (see the supporting information for detail). FIG. S-3 demonstrates single IFNγ sensing microbead can capture 0.0175 pg (= 0.00102 fmol) of IFNγ molecules.

B. Numerical simulation to determine cell secretion rates

By encapsulating single cells with sensing microbeads as well as detection antibodies, we were able to observe the increase in bead fluorescence over time, implying the capturing of cell-secreting targets on beads (FIG. 5). By comparing the calibration curve in FIG. 3 to the fluorescence signals from single cell containing microcompartment, the average amount of cell-secreted cytokines can be roughly

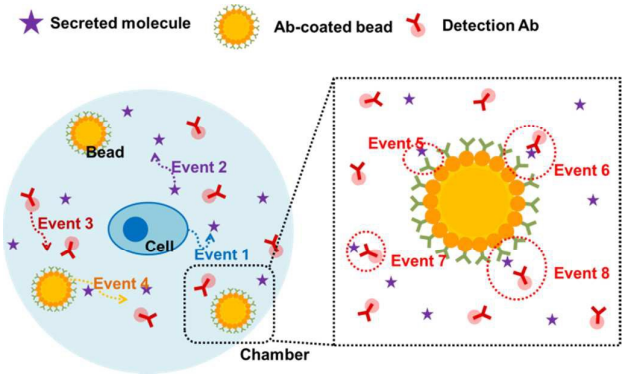

Fig. 4 Drawing describing cellular secretory activities (event 1), the diffusion-based transport of cell-secreting molecules (event 2), detection antibodies (event 3) and sensing beads (event 4), and the binding of those molecules related to detection reaction (event 5 – 8).

estimated at a specific time point. For instance, the estimated average amount of cytokines secreted from single high-secretor (FIG. 5(a)) can be determined to be 0.00030 pg $cell^{-1}$ h^{-1} at t = 6 h and 0.00022 pg $cell^{-1}$ h^{-1} at t = 3 h. Unlike calibration experiment, the concentration of single-cell secreted cytokines varies over time and diffusion of cytokines from cell surface also affects signal, which hinders us from establishing more accurate cell secretion rates. Numerical simulation was performed in this paper to analyze the dynamics of target detection using microbead-incorporating microfluidic system, and to determine the cell secretion rate. We developed a mathematical model accounting for cellular secretory activities, the diffusion-based transport of cell-secreting molecules, detection antibodies and sensing beads, and the binding of those molecules related to detection reaction as illustrated in FIG. 4. A single cell (diameter = 6 μm) confined in a chamber (diameter = 30 μm, height = 30 μm) was assumed to secrete targets at a constant rate, R_{sec} (event 1 in FIG. 4), therefore, the total quantity of targets secreted from the cells can be described as follow:

$$\boldsymbol{n_{Ag} = R_{sec} t} \quad (1)$$

where n_{Ag} is the total number of cell-secreted targets, and *t* is the incubation time. Even though cell secretion rate tends to fluctuate in time[34], this simplified modeling with the assumption of a constant rate may provide useful information for understanding the dynamics of diffusion and detection of targets in the current system.

Free-floating molecules, including cell-secreted molecule (Ag), detection antibody (dAb) and sensing bead (Bead) containing capture antibody (cAb), diffuse inside the closed microcompartment (event 2 – 4):

$$\frac{\partial [Ag]}{\partial t} = \boldsymbol{D_{Ag} \nabla^2 [Ag]} \quad (2)$$

$$\frac{\partial [dAb]}{\partial t} = \boldsymbol{D_{dAb} \nabla^2 [dAb]} \quad (3)$$

$$\frac{\partial [cAb]}{\partial t} = \frac{\partial [Bead]}{\partial t} = \boldsymbol{D_{Bead} \nabla^2 [Bead]} \quad (4)$$

where [*X*] is the concentration of *X* in the chamber and D_X is the diffusion coefficient of *X*. In this study, diffusion of sensing bead is negligible since the concentration of beads is insignificant. When cell-secreted targets (Ag) encounter capture antibodies (cAb) on the bead, they form the target-antibody complex (Ag-cAb) (event 5) as follow:

$$\text{cAb} + \text{Ag} \underset{k_{off1}}{\overset{k_{on1}}{\rightleftharpoons}} \text{cAb-Ag}$$

where k_{on1} and k_{off1} are the association and dissociation constants, respectively. This target-capture antibody complex (cAb-Ag) binds to detection antibody (dAb), forming the product complex, cAb-Ag-dAb, which is closely correlated to signal (event 6):

$$\text{cAb-Ag} + \text{dAb} \underset{k_{off2}}{\overset{k_{on2}}{\rightleftharpoons}} \text{cAb-Ag-dAb (P)}$$

Similarly, the binding reactions between targets (Ag) and detection antibody (dAb) (event 7) and between capture

antibody (cAb) and target-detection antibody complex (Ag-dAb) (event 8) can be described as:

$$\text{Ag} + \text{dAb} \underset{k_{off3}}{\overset{k_{on3}}{\rightleftharpoons}} \text{Ag-dAb}$$

$$\text{cAb} + \text{Ag-dAb} \underset{k_{off4}}{\overset{k_{on4}}{\rightleftharpoons}} \text{cAb-Ag-dAb (P)}$$

For simplifying the simulation, we assumed that binding reaction associated with capture antibody (cAb) takes place in a thin layer (thickness = 20 nm) of streptavidin-biotinylated antibodies formed on the bead's surface, called the reaction region. Therefore, [cAb], [cAb-Ag], and [P] are the concentration of capture antibodies, target-capture antibody complex, and product complex in the reaction region. On the other hand, [Ag], [dAb], and [Ag-dAb] indicate the concentration of target, detection antibody, target-detection antibody complex in the microcompartment.

The binding reactions are modeled by the first-order Langmuir kinetics and can be described as follows:

$$\frac{d[Ag]}{dt} = -k_{on1}[cAb][Ag] + k_{off1}(B_0 - [cAb] - [P]) - k_{on3}[Ag][dAb] + k_{off3}(I_0 - [dAb] - [P]) \quad (5)$$

$$\frac{d[cAb]}{dt} = -k_{on1}[cAb][Ag] + k_{off1}(B_0 - [cAb] - [P]) - k_{on4}[cAb](I_0 - [dAb] - [P]) + k_{off4}[P] \quad (6)$$

$$\frac{d[dAb]}{dt} = -k_{on2}(B_0 - [cAb] - [P])[dAb] + k_{off2}[P] - k_{on3}[Ag][dAb] + k_{off3}(I_0 - [dAb] - [P]) \quad (7)$$

$$\frac{d[P]}{dt} = k_{on2}(B_0 - [cAb] - [P])[dAb] - k_{off2}[P] + k_{on4}[cAb](I_0 - [dAb] - [P]) - k_{off4}[P] \quad (8)$$

where B_0 is the initial concentration of immobilized capture antibodies in the reaction region (total binding sites on beads) and I_0 is the initial concentration of detection antibodies in the chamber. The binding capacity of antibody-functionalized beads was determined by ELISA and fluorescence-based sandwich assay as described in supporting information (FIG. S-3). The equations (1 – 8) were numerically solved to obtain the concentration profile for cell-secreted cytokines and to simulate the rate of cytokine secretion from single cells using COMSOL Multiphysics 4.3. We assumed that 1) convection inside the microcompartment is negligible; and 2) initial concentration of secreted molecules is negligible ($[Ag]_{t=0} = 0$). The values of parameters used in the simulation are summarized in Table 1.

Table 1. Values of parameters used in the simulation

Density of total binding sites, B_0	0.00102 fmol per bead
Concentration of initial detection antibodies, I_0	0.000662 fmol per compartment
Diffusion coefficient of target (IFNγ), D_{Ag}	1.40×10^{-6} cm^2 s^{-1}
Diffusion coefficient of detection antibody, D_{dAb}	5.82×10^{-7} cm^2 s^{-1}
Dissociation binding constant, $K_d = k_{off}/k_{on}$ (estimated)	
Binding between target and capture antibody (#1 and #4)	1nM (k_{on} = 1×10^6 M^{-1} s^{-1}, k_{off} = 1×10^{-3} s^{-1})
Binding between target and detection antibody (#2 and #3)	0.5nM (k_{on} = 2×10^6 M^{-1} s^{-1}, k_{off} = 1×10^{-3} s^{-1})

By assuming cytokine secretion rate R_{sec}, the concentration profile of [P] can be obtained by solving equation (1 – 8), generating theoretical signal which is linearly related to the concentration of [P] in the reaction region. With iterative method to match experimental data to theoretical signal, cytokine secretion rate R_{sec} was determined with a percent root mean square deviation (RMSD) of ~ 5 %.

C. Monitoring cytokine secretion of single CD4$^+$ T cells

Cytokine secretion of single CD4$^+$ T cells was analyzed using our microfluidics containing sensing antibody-beads. CD4$^+$ T cells were isolated from human PBMCs, stained with CellTracker Blue dye to be distinguished from sensing beads, and captured onto the anti-CD4 Ab modified surfaces with a single cell capture efficiency of 45.1 ± 5.8% (two cells = 20.4±3.2%; three cells = 8.8±1.9%; no cell = 22.1±2.7%, n = 655). Next, solution containing mitogens, sensing microbeads and fluorescently-labelled detection antibodies was introduced into the microfluidic device. The vacuum was then released, lowering microcompartments and isolating single cells with sensing beads as well as detection antibodies inside the compartments. Among the chambers encapsulating single T cells (n = 295), 29.8% (n = 88) of chambers contained single sensing beads, 6.1% (n = 18) contained two beads, 1.4% (n = 4) contained three beads, and 62.7% (n = 185) contained no bead, which follows the Poisson distribution (see supporting information for detail). We examined the effects of the number of beads per compartment on the fluorescence signal emanating from one bead to find out if the fluorescence signal is dependent on the number of beads. Our modeling (FIG.S-4) and experiments revealed that per bead fluorescence in multi-bead/single cell compartments was not appreciably different from fluorescence single bead/single cell compartments. This may be explained by the fact that only a small fraction of cytokine molecules are captured on beads and have the detection Ab form sandwich that leads to fluorescence. This observation allowed us to exploit not only the chambers having single cell and single bead but also those having single cell and multibeads for getting information on cytokine secretion, we demonstrated that the number of encapsulated beads might have its least impact on signals using numerical simulation as seen in FIG. S-4. In this paper, therefore, we analyzed the signals from chambers having single cells and at least one bead (n = 110).

We monitored cytokine secretion from mitogenically activated T cells as well as quiescent T cells for 6 h and analyzed the fluorescence intensities of sensing beads. It has been shown previously that stimulation with PMA/Ionomycin stimulation triggers production of cytokines such as IFN-γ from T-cells[35]. Upon stimulation with PMA and ionomycin, 19.1% (n

= 21) of T cells produced high levels of IFN-γ (named 'high-secretor'; T cells showing fluorescence increase of >10 fold above the background at t = 6h) while 80.9% (n = 89) released low levels of this cytokine cells ('low-secretor'; T cells showing fluorescence increase of <10 fold at t = 6h). It is of note that this heterogeneous IFN-γ secretion is consistent with flow cytometry result conducted with commercially available IFN-γ-sensing chimeric antibodies, verifying that there are 17.8% high-secretor and 82.6% low-secretor (see supporting information for the detail). FIG. 5 shows the fluorescence responses of IFN-γ-sensing beads encapsulated with high-secretors, low-secretors, and quiescent cells (individual data: dots; average value: squares; n = 21 for each group). Compared to low-secretors and quiescent cells, high-secretors generated 5-fold and 12-fold higher signal, respectively.

To determine IFN-γ secretion rate, we employed diffusion-reaction model to generate 'theoretical" signal vs. time curves and compare them to actual experimental curves shown in FIG.5(a) using least-squares approximation. Initial secretion rate value entered into the model was determined by IFN-γ ELISA to be 2.67×10^{-5} fmol cell^{-1} h^{-1} (=0.00044 pg cell^{-1} h^{-1}). The secretion rates were determined to be 2.07×10^{-5} fmol cell^{-1} h^{-1} (=0.00035 pg cell^{-1} h^{-1}) for high secretors, 0.45×10^{-5} fmol cell^{-1} h^{-1} for low secretors and 0.18×10^{-5} fmol cell^{-1} h^{-1} for quiescent cells. Theoretical fluorescence signals (dotted lines) generated based on secretion rates for each group were compared to the experimental data (dots) in FIG. 5(a), verifying modeling and experiments to be in close agreement with a percent RMSD of 2.80%, 4.57% and 0.02% for high-secretors, low-secretors, and quiescent cells. It is of note that the secretion rates determined via numerical modeling (0.00035 pg cell^{-1} h^{-1} for high secretor) is comparable to those estimated using calibration curve (0.00030 pg cell^{-1} h^{-1} for high secretor at t = 6 h). Based on estimated IFN-γ release from single cells, we also calculated the average amount of cell-secreted cytokines which were actually captured by sensing beads as well as dAb, thereby generating signals on sensing beads (FIG. 5(b)). FIG. 5(c) shows fluorescence images of sensing beads which were encapsulated not only with stimulated/quiescent single T cells but also with no cells, demonstrating that significant fluorescence signal was observed only with high-secreting stimulated single T cells. In summary, reconfigurable microfluidic device combined with sensing microbeads was used to detect IFN-γ release from single cells after 3 h of stimulation. Importantly, change in signal was monitored over time allowing us to determine secretion rates and the amount of IFN-γ produced by the single cells over the course of the experiment.

D. Monitoring exosome release from single HepG2 cells

We wanted to validate the universality of our device by monitoring the production of nanosized vesicles called 'exosomes' from single cancer cells. Exosomes and vesicles extruded by cells. Exosomes carry a cargo of proteins, RNAs and microRNAs and are capable of regulating gene expression and cellular behavior as well as functions in target cells[36, 37]. For example, exosomes produced by HCC cells have been shown to potentiate inflammation in neighboring cells[38]. There is an increasing interest in developing technologies for exosome detection. However, while a number of approaches have been used for exosome quantification (e.g. Western blot analysis[39], ELISA[40], or SPR-based analysis[41]), real-time monitoring of exosome release and single cell level resolution of exosome release detection of have been difficult to achieve. Therefore, we wanted to demonstrate ability to detect exosomes from single cancer cells using microcompartments and entrapped sensing beads.

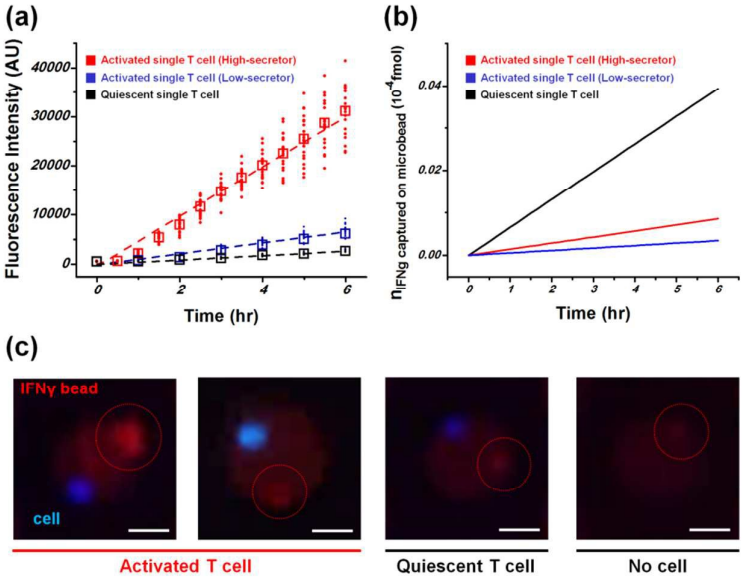

Fig. 5 Real-time detection of IFN-γ secretion from single CD4$^+$ T cells and numerical simulation of IFN-γ secretion and diffusion over time based on the diffusion-reaction modeling. (a) Comparison of simulation results (dotted lines) with experimental data (dots) showing change in fluorescence increase over time for high-secreting stimulated single cells (red), low-secreting stimulated single cells (blue), and quiescent cells (black) (n = 21 for each group). (b) Simulation results showing the average amount of cell-secreted IFN-γ captured by sensing microbeads over time for high-secretors (red), low-secretors (blue), and quiescent cells (black). (c) Fluorescence images of chambers having IFN-γ sensing beads (red) and stimulated/quiescent single T cells (blue) after 6 h of incubation. Scale bar = 10 μm.

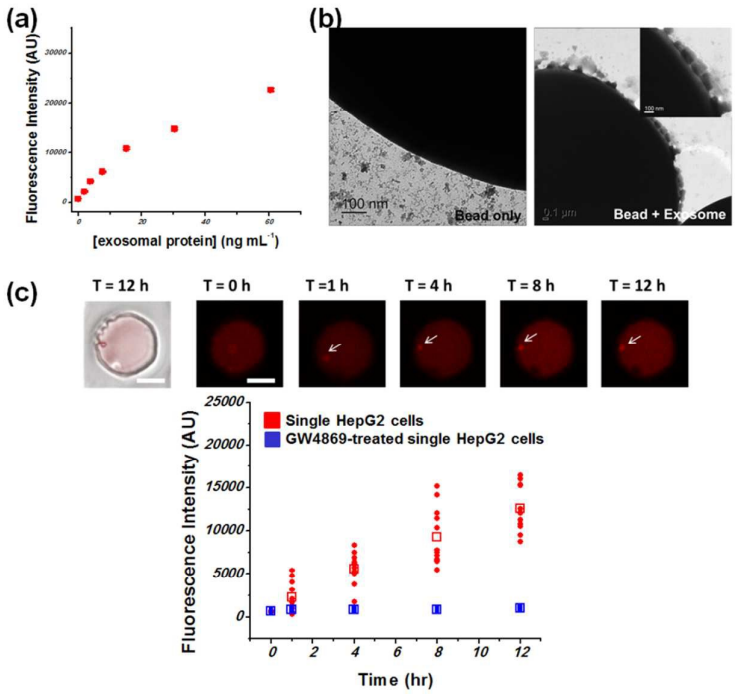

Fig. 6 Real-time detection of exosome production from single HepG2 cells. (a) Calibration curve with isolated exosomes. Fluorescence intensities of anti-CD63 cAb-beads (10^6 particles mL^{-1}) after incubating with varying concentrations of isolated exosomes (conc. of exosomal protein = 0 – 60 ng mL^{-1}) and PE-labelled anti-CD63 dAb (conc. = 5 µg mL^{-1}) for 3 hr. The concentration of isolated exosomes was determined by BCA assay. (b) Transmission electron microscopic images of bead (negative control) and bead incubated with isolated exosomes for 3 hr. (c) Time-lapse fluorescent images of anti-CD63 cAb-bead over time for single HepG2 cell encapsulated in chambers (Scale bar = 20 µm) and fluorescence change over time for single HepG2 cells (red, n = 12) and single GW4869-treated HepG2 cells (blue, n = 7).

Microbeads were functionalized with Abs against CD63, one of the most abundant transmembrane proteins found on exosomes. Microbeads conjugated with biotinylated anti-CD63 cAbs (10^6 particles mL^{-1}) were challenged with different concentrations of exosomal protein content (0 to 60 ng mL^{-1}) and 5 µg mL^{-1} of PE-labelled detection antibodies (dAb) for 3 h. FIG. 6(a) displays the fluorescence response of exosome-sensing beads with linear range extending to 60 ng mL^{-1} (R^2 = 0.904) and the LOD of 3.3 ng mL^{-1}. The capture of exosomes by beads was visualized using transmission electron microscopy (TEM). FIG. 6(b) demonstrates presence of exosomes on a representative microbead after 3h incubation inside a microcompartment containing single cancer cell.

Furthermore, exosome production of single cancer cells was monitored over time as shown in FIG. 6(c). As a negative control, HepG2 cells were treated with 10 µM GW4869, an agent that inhibits exosome production but does not cause cytotoxicity in the short term[42]. HepG2 cells were captured on 40 µm diameter islands patterned on the floor of the microfluidic device and then incubated with anti-CD63 cAb-beads as well as PE-labelled anti-CD63 dAbs for 12 h. FIG. 6(c) shows change in fluorescence signal due to capture of exosomes from single HepG2 cells, indicating that exosome production from single HepG2 cells occurs in heterogeneous manner. Additional fluorescence images of beads and single cells were shown in FIG. S6. Importantly, change in fluorescence did not occur when HepG2 cells were pretreated with GW4869 (FIG. 6(c)). We estimated the average amount of cell-secreted exosomes captured on the sensing beads by comparing the fluorescence signals from cells (FIG. 6(c)) to those from isolated exosomes (FIG. 6(a)).

Limited information on exosomes, such as molecular weight, binding site density, association/dissociation constants hampered modeling of exosome secretion dynamics. Therefore, we estimated the average quantity of exosomes secreted by single HepG2 cells over the course of 12 h using calibration curve. For better fitting, the log-log model was applied to the calibration curve (R^2=0.995). This quantity of exosomes was based on the protein content and was estimated to be 0.92±0.29 fg. We previously determined protein content to vary from 10.4 to 53.4 ng per 10^7 particles (data not shown), indicating that the average amount of exosomes secreted from single HepG2 cells after 12 h was $(0.17 – 0.89)\times10^2$ particles.

Conclusions

This paper describes the use of reconfigurable microfluidics and sensing microbeads for dynamic monitoring of lipid particles (exosomes) or proteins released from single cells. Ab-functionalized microbeads were co-entrapped with single cells inside picoliter scale microcompartments. Fluorescently-labeled secondary Abs were also present inside the microcompartments. As secreted cytokines or exosomes became captured on the microbeads, secondary Abs attached to the microbeads causing bead fluorescence to increase as a

function of time. We demonstrated utility of this strategy for the detection of IFN-γ release from single T-cells and exosome secretion from single cancer cells. In the future, this approach may be extended to detect multiple cell-secreted signals and may be combined with cell retrieval to enable function-based sorting of single cells.

Acknowledgements

Financial support for this work was provided by grants from the NSF. In addition, we gratefully acknowledge the funding provided by "Research Investments in Science and Engineering from UC Davis."

References

1. R. Zenobi, *Science*, 2013, **342**, 1243259.
2. R. Satija and A. K. Shalek, *Trends in immunology*, 2014, **35**, 219-229.
3. S. J. Altschuler and L. F. Wu, *Cell*, 2010, **141**, 559-563.
4. A. M. Malyguine, S. Strobl, K. Dunham, M. R. Shurin and T. J. Sayers, *Cells*, 2012, **1**, 111-126.
5. A. J. Torres, A. S. Hill and J. C. Love, *Analytical chemistry*, 2014, **86**, 11562-11569.
6. T. Sun, J. Kovac and J. Voldman, *Analytical chemistry*, 2014, **86**, 977-981.
7. H. Zhu, G. Stybayeva, J. Silangcruz, J. Yan, E. Ramanculov, S. Dandekar, M. D. George and A. Revzin, *Analytical Chemistry*, 2009, **81**, 8150-8156.
8. V. Chokkalingam, J. Tel, F. Wimmers, X. Liu, S. Semenov, J. Thiele, C. G. Figdor and W. T. S. Huck, *Lab on a chip*, 2013, **13**, 4740-4744.
9. D. Di Carlo, L. Y. Wu and L. P. Lee, *Lab on a chip*, 2006, **6**, 1445-1449.
10. E. J. Smith, S. Schulze, S. Kiravittaya, Y. F. Mei, S. Sanchez and O. G. Schmidt, *Nano Lett*, 2011, **11**, 4037-4042.
11. J. H. Choi, A. O. Ogunniyi, M. D. Du, M. N. Du, M. Kretschmann, J. Eberhardt and J. C. Love, *Biotechnol Progr*, 2010, **26**, 888-895.
12. B. D. Plouffe, M. A. Brown, R. K. Iyer, M. Radisic and S. K. Murthy, *Lab on a chip*, 2009, **9**, 1507-1510.
13. D. S. Shin, J. You, A. Rahimian, T. Vu, C. Siltanen, A. Ehsanipour, G. Stybayeva, J. Sutcliffe and A. Revzin, *Angew Chem Int Edit*, 2014, **53**, 8221-8224.
14. K. J. Son, D. S. Shin, T. Kwa, J. You, Y. Gao and A. Revzin, *Lab on a chip*, 2015, **15**, 637-641.
15. W. S. Yeo, M. N. Yousaf and M. Mrksich, *J Am Chem Soc*, 2003, **125**, 14994-14995.
16. C. Ma, R. Fan, H. Ahmad, Q. Shi, B. Comin-Anduix, T. Chodon, R. C. Koya, C. C. Liu, G. A. Kwong, C. G. Radu, A. Ribas and J. R. Heath, *Nature medicine*, 2011, **17**, 738-743.
17. N. Varadarajan, B. Julg, Y. J. Yamanaka, H. B. Chen, A. O. Ogunniyi, E. McAndrew, L. C. Porter, A. Piechocka-Trocha, B. J. Hill, D. C. Douek, F. Pereyra, B. D. Walker and J. C. Love, *J Clin Invest*, 2011, **121**, 4322-4331.
18. Y. Lu, J. J. Chen, L. Y. Mu, Q. Xue, Y. Wu, P. H. Wu, J. Li, A. O. Vortmeyer, K. Miller-Jensen, D. Wirtz and R. Fan, *Analytical chemistry*, 2013, **85**, 2548-2556.
19. L. Mazutis, J. Gilbert, W. L. Ung, D. A. Weitz, A. D. Griffiths and J. A. Heyman, *Nat Protoc*, 2013, **8**, 870-891.
20. T. Konry, A. Golberg and M. Yarmush, *Scientific reports*, 2013, **3**.
21. A. Cattamanchi, R. Smith, K. R. Steingart, J. Z. Metcalfe, A. Date, C. Coleman, B. J. Marston, L. Huang, P. C. Hopewell and M. Pai, *Jaids-J Acq Imm Def*, 2011, **56**, 230-238.
22. M. Logozzi, A. De Milito, L. Lugini, M. Borghi, L. Calabro, M. Spada, M. Perdicchio, M. L. Marino, C. Federici, E. Iessi, D. Brambilla, G. Venturi, F. Lozupone, M. Santinami, V. Huber, M. Maio, L. Rivoltini and S. Fais, *PloS one*, 2009, **4**, e5219.
23. H. W. King, M. Z. Michael and J. M. Gleadle, *BMC cancer*, 2012, **12**, 421.
24. A. Bobrie, M. Colombo, G. Raposo and C. Thery, *Traffic*, 2011, **12**, 1659-1668.
25. G. Raposo and W. Stoorvogel, *J Cell Biol*, 2013, **200**, 373-383.
26. J. Skog, T. Wurdinger, S. van Rijn, D. H. Meijer, L. Gainche, M. Sena-Esteves, W. T. Curry, Jr., B. S. Carter, A. M. Krichevsky and X. O. Breakefield, *Nature cell biology*, 2008, **10**, 1470-1476.
27. W.-h. Liu, L.-n. Ren, X. Wang, T. Wang, N. Zhang, Y. Gao, H. Luo, N. Navarro-Alvarez and L.-j. Tang, *J Cancer Res Clin Oncol*, 2015, DOI: 10.1007/s00432-015-1943-0, 1-12.
28. S. Lemoinne, D. Thabut, C. Housset, R. Moreau, D. Valla, C. M. Boulanger and P. E. Rautou, *Nat Rev Gastro Hepat*, 2014, **11**.
29. M. A. Unger, H. P. Chou, T. Thorsen, A. Scherer and S. R. Quake, *Science*, 2000, **288**, 113-116.
30. B. Mosadegh, C. H. Kuo, Y. C. Tung, Y. S. Torisawa, T. Bersano-Begey, H. Tavana and S. Takayama, *Nature physics*, 2010, **6**, 433-437.
31. J. M. Street, P. E. Barran, C. L. Mackay, S. Weidt, C. Balmforth, T. S. Walsh, R. T. A. Chalmers, D. J. Webb and J. W. Dear, *J Transl Med*, 2012, **10**.
32. J. L. Welton, S. Khanna, P. J. Giles, P. Brennan, I. A. Brewis, J. Staffurth, M. D. Mason and A. Clayton, *Mol Cell Proteomics*, 2010, **9**, 1324-1338.
33. G. L. Long and J. D. Winefordner, *Analytical chemistry*, 1983, **55**, A712-&.
34. Y. Gao, Q. Zhou, Z. Matharu, Y. Liu, T. Kwa and A. Revzin, *Biomicrofluidics*, 2014, **8**, 021501.
35. I. Olsen and L. M. Sollid, *J Immunol Methods*, 2013, **390**, 106-112.
36. H. Valadi, K. Ekstrom, A. Bossios, M. Sjostrand, J. J. Lee and J. O. Lotvall, *Nat Cell Biol*, 2007, **9**, 654-U672.
37. G. Camussi, M. C. Deregibus, S. Bruno, C. Grange, V. Fonsato and C. Tetta, *Am J Cancer Res*, 2011, **1**, 98-110.
38. T. Kogure, W. L. Lin, I. K. Yan, C. Braconi and T. Patel, *Hepatology*, 2011, **54**, 1237-1248.
39. G. van Niel, G. Raposo, C. Candalh, M. Boussac, R. Hershberg, N. Cerf-Bensussan and M. Heyman, *Gastroenterology*, 2001, **121**, 337-349.
40. M. Logozzi, A. De Milito, L. Lugini, M. Borghi, L. Calabro, M. Spada, M. Perdicchio, M. L. Marino, C. Federici, E. Iessi, D. Brambilla, G. Venturi, F. Lozupone, M. Santinami, V. Huber, M. Maio, L. Rivoltini and S. Fais, *PloS one*, 2009, **4**.
41. H. Im, H. L. Shao, Y. I. Park, V. M. Peterson, C. M. Castro, R. Weissleder and H. Lee, *Nature biotechnology*, 2014, **32**, 490-U219.
42. J. Li, K. Liu, Y. Liu, Y. Xu, F. Zhang, H. Yang, J. Liu, T. Pan, J. Chen, M. Wu, X. Zhou and Z. Yuan, *Nature immunology*, 2013, **14**, 793-803.